Density Matrix Renormalization Group for Continuous Quantum Systems

Shovan Dutta,[1,2,3] Anton Buyskikh,[4] Andrew J. Daley,[4] and Erich J. Mueller[2]
[1]T.C.M. Group, Cavendish Laboratory, University of Cambridge, JJ Thomson Avenue, Cambridge CB3 0HE, United Kingdom
[2]Laboratory of Atomic and Solid State Physics, Cornell University, Ithaca, New York 14853, USA
[3]Max Planck Institute for the Physics of Complex Systems, 01187 Dresden, Germany
[4]Department of Physics and SUPA, University of Strathclyde, Glasgow G4 0NG, United Kingdom

(Received 20 August 2021; revised 22 March 2022; accepted 6 May 2022; published 8 June 2022)

We introduce a versatile and practical framework for applying matrix product state techniques to continuous quantum systems. We divide space into multiple segments and generate continuous basis functions for the many-body state in each segment. By combining this mapping with existing numerical density matrix renormalization group routines, we show how one can accurately obtain the ground-state wave function, spatial correlations, and spatial entanglement entropy directly in the continuum. For a prototypical mesoscopic system of strongly interacting bosons we demonstrate faster convergence than standard grid-based discretization. We illustrate the power of our approach by studying a superfluid-insulator transition in an external potential. We outline how one can directly apply or generalize this technique to a wide variety of experimentally relevant problems across condensed matter physics and quantum field theory.

DOI: 10.1103/PhysRevLett.128.230401

Few computational techniques have improved our understanding of strongly correlated quantum systems as much as the density matrix renormalization group (DMRG) [1]. The DMRG takes advantage of the entanglement properties of many one-dimensional (1D) physical states [2] to efficiently truncate the Hilbert space, approximating the many-body wave function as a variational matrix product state (MPS). It has been successfully generalized for time evolution [3] and is the method of choice for simulating *discrete* 1D quantum systems, with promising extensions to higher dimensions and other tensor networks [4]. However, despite wide-ranging potential applications [5–8], attempts to generalize the DMRG to continuous systems have encountered substantial difficulties. Here, we present a new framework that addresses this long-standing challenge.

Tensor-network approaches require a lattice. To apply them to continuous systems one must define a network of local Hilbert spaces. The naive approach involves replacing the continuum with a lattice [9–11]. Unfortunately, this strategy scales poorly with the number of grid points and displays convergence issues in systems with multiple length scales [12,13], requiring optimization on successively finer grids [13–15], which becomes intractable for vanishingly small grid spacing [16]. Alternatively, by taking this continuum limit one can derive a field-theoretic description, called continuous MPS (cMPS) [17], which has had considerable success for translationally invariant systems [18–22] but faces challenges in the presence of inhomogeneities, requiring sufficiently preconverged initial states to avoid instabilities [23]. New ansatzes may solve some of these challenges [24]. Regardless, cMPS calculations are intrinsically nonlinear [25,26], and it is not generally known how to encode symmetries such as particle-number conservation [17,27].

In contrast, we partition a continuous system into multiple *segments* and choose a flexible set of basis functions in each segment to describe the local physics. This recipe turns the Hamiltonian into a sum over segments, with nearest-neighbor terms imposing continuity at the boundaries. This form can be minimized using standard DMRG routines [28], used as a local basis for other tensor network algorithms, or even used for neural-network based approaches [29]. Like a Hubbard Hamiltonian, one can easily incorporate symmetries [30] such as particle number, and the method works equally well for homogeneous and inhomogeneous systems, regardless of the initial state. For many segments and few basis functions, it reduces to discretizing on a grid; however, we show that for interacting bosons in a box one can optimize the local basis to gain faster convergence with a small number of segments. We illustrate the broad applicability of this technique by exploring the Mott-superfluid transition in a sinusoidal potential.

For concreteness, we consider a paradigmatic Hamiltonian describing N bosons with contact interactions [31] trapped in a box of length L,

$$\hat{H} = \int_0^L dx \left[\frac{1}{2} \frac{d\hat{\psi}^\dagger}{dx} \frac{d\hat{\psi}}{dx} + \frac{g}{2} \hat{\psi}^\dagger \hat{\psi}^\dagger \hat{\psi} \hat{\psi} + V(x) \hat{\psi}^\dagger \hat{\psi} \right], \quad (1)$$

where $\hat{\psi}(x)$ is the boson field operator, g is the interaction strength, $V(x)$ is an external potential, and we have set $\hbar = m = 1$, where m is the boson mass. This 1D model is realized for atoms with tight transverse confinement [32,33], with optical box traps [34] or atom chips [35,36]. Its physics depends crucially on the ratio of interaction and kinetic energies, set by the dimensionless parameter $\gamma := gL/N$. When $V(x) = 0$, the model has an exact Bethe-ansatz solution [37–39], but calculating spatial correlations is challenging except for $\gamma \ll 1$ [40] and $\gamma \to \infty$ [41]. Thus, one typically resorts to low-energy approximations [42] or, in static cases, Monte Carlo simulations [43].

To use standard DMRG techniques, one can discretize Eq. (1) on a grid of spacing ϵ, mapping $\hat{\psi}$ to lattice bosons, $\hat{\psi}(x) \to \hat{b}_i/\sqrt{\epsilon}$, and replacing derivatives by finite differences, which gives [44]

$$\hat{H} \approx -\frac{1}{2\epsilon^2} \sum_{\langle i,j \rangle} \hat{b}_i^\dagger \hat{b}_j + \sum_{j=1}^{M-1} \frac{g}{2\epsilon} \hat{b}_j^\dagger \hat{b}_j^\dagger \hat{b}_j \hat{b}_j + \left(V_j + \frac{1}{\epsilon^2} \right) \hat{b}_j^\dagger \hat{b}_j, \quad (2)$$

where $\langle i, j \rangle$ denotes nearest neighbors and $M - 1$ is the number of grid points in the bulk, $L = M\epsilon$; see Ref. [14] for an alternative mapping to hard-core bosons. The continuum limit is obtained for $M \to \infty$.

Instead, we divide the box into M finite segments with

$$\hat{\psi}(x) = \sum_{j=1}^{M} \square_{X_{j-1}, X_j}(x) \hat{\psi}(x), \quad (3)$$

where the box function $\square_{a,b}(x)$ vanishes unless $a \le x < b$; $\square_{a,b}(x) := \theta(x - a) - \theta(x - b)$, with θ denoting the unit step function. Thus, X_j is the boundary between the jth and the $(j + 1)$th segments, with $X_0 = 0$ and $X_M = L$. Substituting Eq. (3) into Eq. (1) and keeping track of delta functions, we find (see Supplemental Material [45])

$$\hat{H} = \sum_{j=1}^{M} \hat{K}_j + \hat{U}_j + \hat{P}_j + \Lambda \sum_{j=0}^{M} \hat{\Upsilon}_{j,j+1}, \quad (4)$$

where $\hat{K}_j$, $\hat{U}_j$, and $\hat{P}_j$ are, respectively, the kinetic, interaction, and potential energies in the jth segment, given by integrals between X_{j-1} and X_j, and

$$\hat{\Upsilon}_{j,j+1} := [\hat{\psi}(X_j^-) - \hat{\psi}(X_j^+)]^\dagger [\hat{\psi}(X_j^-) - \hat{\psi}(X_j^+)] \quad (5)$$

is a positive-semidefinite measure of the discontinuity between $x \to X_j^-$ and $x \to X_j^+$. We use hard-wall boundary conditions at the edges of our system, and in Eq. (5) define $\hat{\psi}(0^-) := \hat{\psi}(L^+) := 0$. The prefactor Λ is a formally infinite energy penalty that projects onto continuous states,

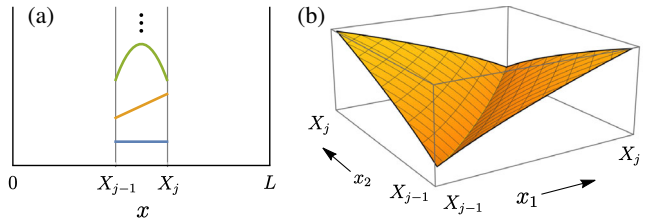

FIG. 1. Examples of (a) one-body and (b) two-body basis functions in a segment between X_{j-1} and X_j. The cusp at $x_1 = x_2$ in (b) encodes the physics of contact interactions.

"gluing" the segments together. In our numerical calculations, we take Λ to be finite, increasing it in consecutive DMRG cycles. This approach accelerates convergence because the system takes larger steps through phase space when Λ is smaller.

Equation (4) has the form of a Hubbard model, with "on-site" and nearest-neighbor terms. It can be expressed as a compact matrix product operator (MPO) [1] once we select n-body basis functions $\phi_{n,k}^{(j)}(\vec{r})$ in each segment j, where $n = 0, 1, \ldots$ up to some cutoff $n_{\max} \le N$, and k labels the different states for a given n. The construction of these basis functions is described below and examples of one- and two-particle states are shown in Fig. 1. In contrast, for a lattice model as in Eq. (2), the local bases are simply labeled by the number of particles on each site, $|0\rangle_j, \ldots, |n_{\max}\rangle_j$. Once our continuous bases are chosen, one calculates matrix elements

$$\langle \phi_{n-1,k}^{(j)} | \hat{\psi}(x) | \phi_{n,k'}^{(j)} \rangle = \sqrt{n} \int_{X_{j-1}}^{X_j} d^{n-1} r \phi_{n-1,k}^{(j)*}(\vec{r}) \phi_{n,k'}^{(j)}(x, \vec{r}),$$

where $x \in [X_{j-1}, X_j]$ and $n \ge 1$. Similar expressions for the matrix elements of $\hat{K}_j$, $\hat{U}_j$, and $\hat{P}_j$ are derived in the Supplemental Material [45]. Note these operators conserve particle number and are thus block diagonal. If we choose the segments to have equal width, then the basis functions on different segments can be translations of one another, and the local matrices become independent of j.

We take the basis functions to be piecewise polynomials, i.e., for $X_{j-1} \le x_1 \le x_2 \le \ldots \le x_n \le X_j$, $\phi_{n,k}^{(j)}(\vec{R}_{j-1} + \vec{r}) = \sum_{\mathbf{p}} A_{n,k,\mathbf{p}}^{(j)} x_1^{p_1} \ldots x_n^{p_n}$, and the other sectors are determined by symmetry under particle exchange. Here, $\mathbf{p} = \{p_1, \ldots, p_n\}$ is a vector of the powers that appear in each monomial. As a practical strategy, we limit the maximum degree of the monomials: $p_1 + \cdots + p_n \le d_{\max}$, which means one can approximate the wave function as a Taylor series of order $d_{\max}$ in each symmetry sector. We choose $A_{n,k,\mathbf{p}}^{(j)}$ so that the basis is orthonormal, $\langle \phi_{n,k}^{(j)} | \phi_{n,k'}^{(j)} \rangle = \delta_{k,k'}$. Given these constraints, we wish to construct polynomials that capture the low-energy physics with a minimum number of states. For example, the contact interaction in Eq. (1) gives rise to a kink in the wave function wherever two particles coincide [31], $\partial_{x_i} \Psi(x_i \to x_{i'}^+) - \partial_{x_i} \Psi(x_i \to x_{i'}^-) = g\Psi(x_i = x_{i'})$.

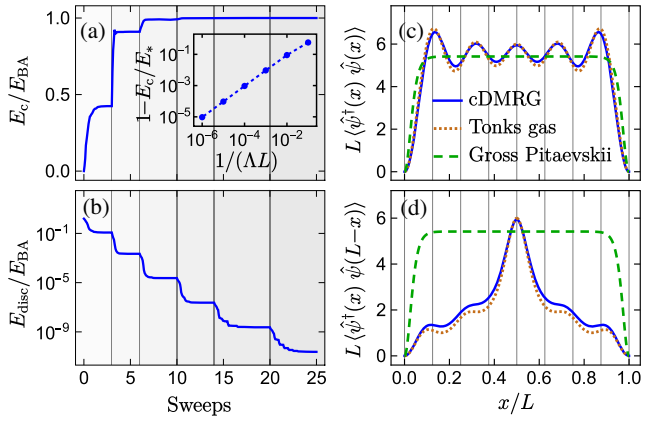

FIG. 2. Ground-state calculation for 5 bosons with strong interactions ($\gamma = 50$) in a uniform box, divided into 8 segments. (a),(b) Starting from a localized state, as the penalty Λ is increased in powers of 10, the discontinuity falls as $1/\Lambda^2$ and the energy approaches the asymptotic value E_*, which is within 5×10^{-6} of the exact Bethe-ansatz result E_{BA}. (The remaining discrepancy is due to the finite basis set used.) Here, $E_c = \sum_j \langle \hat{K}_j + \hat{U}_j \rangle$ and $E_{\mathrm{disc}} \coloneqq (N/L) \sum_j \langle \hat{\Upsilon}_{j,j+1} \rangle$ [see Eqs. (4)–(5)]. The inset shows E_c approaching E_* as $1/\Lambda$. (c),(d) Density and correlations in the ground state, showing Friedel oscillations similar to exact results for the Tonks gas ($\gamma \to \infty$) and far from a mean-field Gross-Pitaevskii theory. The mismatch between the cDMRG and Tonks curves is due to the different values of γ. See Supplemental Material [45] for a full description of the basis states and the DMRG parameters.

The numerics are more efficient if we include the same kink in the basis functions $\phi^{(j)}_{n,k}(\vec{r})$. In the Supplemental Material [45], we show how to construct generalizations of Legendre polynomials that possess these cusps. Calculating the local basis, and the matrix elements of the local operators, only needs to be done once and makes a negligible contribution to the computation time, which is dominated by the DMRG sweeps.

With this construction, the matrix elements of local operators become piecewise polynomial functions of the form $\langle \phi^{(j)}_{n,k} | \hat{\mathcal{F}}(x) | \phi^{(j)}_{m,k'} \rangle = \sum_{p=0}^{p_{\max}} F^{j,p}_{nk,mk'} (x - X_{j-1})^p$. Thus, one can evaluate spatial correlations $\langle \hat{\mathcal{F}}^\dagger(x) \hat{\mathcal{F}}(x') \rangle$ at any point once the matrices $F^{j,p}$ are stored.

Clearly, there is a tradeoff between the basis size set by $\{n_{\max}, d_{\max}\}$ and the number of partitions M. In practice, it is sufficient to choose $n_{\max} \gg N/M$ and increase M for a given $d_{\max}$ to recover the true continuum limit. See Supplemental Material [45] for a more detailed discussion of the convergence parameters.

Figure 2 shows a benchmark calculation for $N = 5$ strongly interacting bosons in a uniform trap [$V(x) = 0$], divided into $M = 8$ equal segments with basis functions that can describe quartic variations, i.e., $d_{\max} = 4$. We initialize the particles in a discontinuous product state, where each segment contains either zero or one particle, and the single-particle wave function is uniform, hence $E_c \coloneqq \sum_j \langle \hat{K}_j + \hat{U}_j \rangle = 0$. We use the standard DMRG algorithm to minimize $\hat{H}$ in Eq. (4) with a small penalty Λ. As shown in Figs. 2(a)–2(b), E_c increases with each sweep, and the discontinuity drops. After convergence, we sequentially increase Λ by factors of 10, stopping when the discontinuity falls below a small threshold. For large Λ, the energy saturates at $E_c \approx E_* - \eta/\Lambda$ with constant η, from which one can robustly extrapolate E_*. Already with $M = 8$, E_* matches the ground-state energy from Bethe ansatz [38] to 5×10^{-6}. The density in Fig. 2(c) shows oscillations that are similar to those found in the Tonks gas, which would model the system for $\gamma \to \infty$ [41]. In that limit, these corrugations can be interpreted as the Friedel oscillations of a free Fermi gas [39], which are not reproduced in mean-field theory [40]. Similarly, the single-particle correlator in Fig. 2(d) has a peak at small distances, and distinctive steps. The Luttinger-liquid power-law tail is cut off by hard-wall boundaries [42]. We capture the correlations down to arbitrarily small distances, and thus recover the $1/\kappa^4$ tail in the momentum distribution $n(\kappa)$ (see Supplemental Material [45]), characteristic of contact interactions [47].

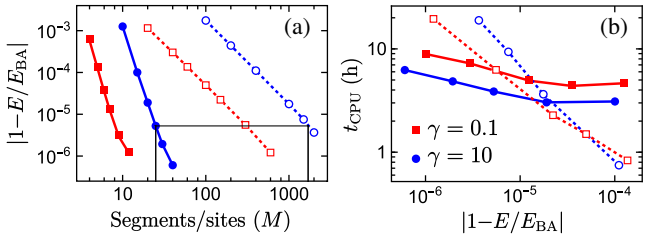

FIG. 3. (a) Relative error vs number of segments (grid points) and (b) CPU time vs relative error in finding ground states for $N = 10$ using cDMRG (solid lines) and discretization on a grid (dotted lines). For cDMRG, E is the extrapolated energy $E_* > E_{\mathrm{BA}}$ (see Fig. 2). We retained up to cubic basis functions in each segment, causing the error to fall off as M^{-6}, instead of M^{-2} for discretization. Empirically, $t_{\mathrm{CPU}} \sim |1 - E/E_{\mathrm{BA}}|^{-0.2}$ for cDMRG at small errors, whereas for discretization this exponent is -0.75 for $\gamma = 0.1$ and -1 for $\gamma = 10$. Note, t_{CPU} was measured in seconds from the number of clock cycles during all DMRG sweeps on single quad-core CPUs. The saturation at large errors in (b) is due to larger bond dimensions [45].

Figure 3 explores the performance of our algorithm, continuous DMRG (cDMRG), and compares it with the grid-based discretization in Eq. (2). We consider $N = 10$ particles and piecewise cubic basis states ($d_{\max} = 3$). As illustrated by panel (a), as one refines the grid, the error in ground-state energy falls off as $M^{-2d_{\max}}$: The energy per segment can be approximated up to that order. The standard discretization instead shows an error scaling as M^{-2}. Increasing $d_{\max}$ allows one to achieve the same accuracy with fewer segments, at the cost of a larger basis. The relationship between CPU time and accuracy is shown in

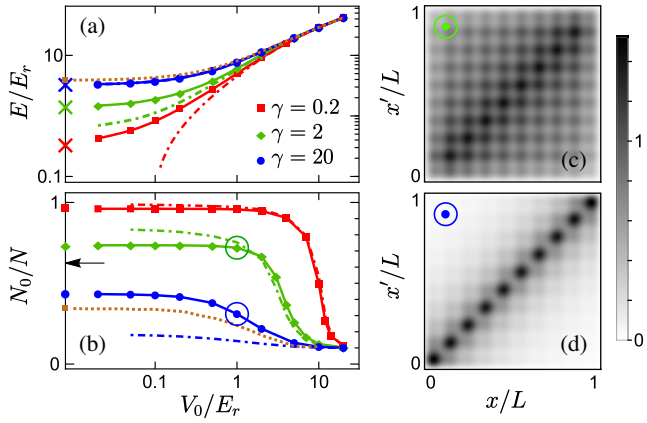

FIG. 4. (a) Ground-state energy and (b) condensate fraction for 10 bosons in 10 potential wells of depth V_0 using cDMRG with 20 segments and quartic basis functions (solid lines) and using a tight-binding approximation (dash-dotted lines). Here, N_0 is the occupation of the single-particle ground state. Dotted lines in (a),(b) and crosses in (a) show exact solutions for the Tonks gas and from Bethe ansatz, respectively; the condensate fractions are found using Monte Carlo integration [45]. The arrow in (b) marks the N_0 for $\gamma \approx 4.22$, when the ground state for $V_0 \to 0$ becomes Mott insulating. In our finite-size system this transition is a crossover. (c),(d) Single-particle correlations, $\langle \hat{\psi}^\dagger(x)\hat{\psi}(x')\rangle L/N$, in a superfluid and a Mott state, corresponding to circled points in (b) [45].

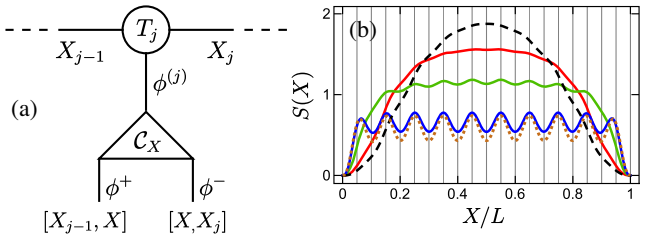

FIG. 5. (a) Schematic of how one can decompose a tensor T_j of the MPS by a basis splitting $\phi^{(j)} \to \phi^+ \otimes \phi^-$ to calculate the entanglement between arbitrary bipartitions $[0, X]$ and $[X, L]$. (b) Ground-state entanglement entropy for 10 bosons in a shallow lattice ($V_0 = E_r$) with interactions $\gamma = 0.2$ (red), 2 (green), 20 (blue), using cDMRG with the same numerical parameters as in Fig. 4. We have split each segment at 20 intermediate points [45]. Dashed and dotted curves show exact results for $\gamma = 0$ [50] and $\gamma \to \infty$ [48], respectively.

Fig. 3(b). The traditional discretization is more efficient for low-accuracy calculations, where the smaller local Hilbert space is beneficial. Our algorithm uses fewer computational resources for high-accuracy calculations, where precise modeling of the local physics is crucial. The crossover point depends on the interaction strength: cDMRG is more efficient for strong repulsive interactions, which suppress the occupation of basis states containing more particles. Similarly, the error in the single-particle correlations decays as $M^{-(d_{\max}+1)}$ [45].

Since the ground-state entanglement entropy of this system grows as $\ln N$ [48–50], we find a linear rise in the DMRG bond dimension [51] with particle number, and the computation time roughly scales as N^3 [1]. Our calculations were done using the ITensor library [28], using a two-site DMRG algorithm with a singular-value cutoff of 10^{-14}, resulting in bond dimensions of order 100 (see Supplemental Material [45] for details).

Next, we consider $V(x) = V_0 \cos^2(N_w \pi x/L)$, with N_w potential wells between 0 and L, which makes the system nonintegrable. There are two simple limits: (i) For $V_0 \gg E_r = N_w^2 \pi^2/(2L^2)$, where E_r is the recoil energy, a tight-binding approximation reduces the problem to a Bose-Hubbard model with N_w sites and slightly nonuniform parameters [45]. (ii) For $\gamma \to \infty$, the system maps onto free fermions [52]. Figure 4(a) shows how the cDMRG reproduces these limits and smoothly connects the tight-binding and Bethe-ansatz regimes for all γ. For $N_w = N$, we find signatures of the superfluid-to-Mott-insulator transition [53] for both deep ($V_0 \gg E_r$) and shallow lattices ($V_0 \sim E_r$): As γ is increased, the ground-state coherences localize, i.e., the algebraic variation of the correlation functions [Fig. 4(c)] becomes exponential [Fig. 4(d)], accompanied by a drop in the condensate fraction [Fig. 4(b)]. Similar to unbounded systems [54,55] and those with periodic boundary conditions [56,57], the low-energy physics for $V_0 \to 0$ is described by a quantum sine-Gordon Hamiltonian [58], which gives a Mott phase for $\gamma > \gamma_c \approx 3.5 + 7.5/N$ (see Supplemental Material [45]). Hence, the superfluid phase is found only for $\gamma < \gamma_c$ and sufficiently small V_0.

Crucially, our approach allows one to compute the spatial bipartite entanglement entropy S directly in the continuum. To form a bipartition at an arbitrary position $X \in (X_{j-1}, X_j)$, we divide the jth segment into left and right zones, with their own basis functions $\phi^{\pm}_{n,k}$, and write the original basis as a tensor product, $\phi^{(j)}_{n,k} = \sum_{n',k^\pm} \mathcal{C}^{n,k}_{n',k^+,k^-} \phi^+_{n',k^+} \phi^-_{n-n',k^-}$ [45]. Thus, one expresses the local tensor T_j of the MPS in the product basis [Fig. 5(a)], and calculates $S(X)$ via a Schmidt decomposition [1]. For bipartition at a segment boundary, the subdivision step can be skipped. Figure 5(b) shows the entropy variation in a shallow lattice. At weak coupling, where there are large number fluctuations, the entropy is peaked about the center, characteristic of the critical superfluid phase [59]. In contrast, at strong coupling the entropy is largely flat, corresponding to the short-range "area-law" entanglement expected in the Mott phase [2]. Additionally, there are small wiggles that are related to Friedel oscillations [Fig. 2(c)]. This spatial variation can be measured in current experiments [7] and used as a tool to characterize continuous phases.

Finally, we give examples of how our framework can be applied more generally. First, for multicomponent bosons with contact interactions [5], one can partition each component σ into the same segments, altering Eq. (4) to

$$\hat{H} = \sum_j \left[\sum_\sigma \hat{K}_j^\sigma + \hat{P}_j^\sigma + \Lambda \hat{\Upsilon}_{j,j+1}^\sigma + \sum_{\sigma,\sigma'} \hat{U}_j^{\sigma,\sigma'} \right], \quad (6)$$

which still has only on-site and nearest-neighbor terms and thus the same MPO bond dimension. The basis functions will carry additional labels to accommodate all the components, e.g., $\phi^{(j)}_{n^\uparrow,n^\downarrow,k}$ for $\sigma = \uparrow, \downarrow$. The pairwise interaction strengths will determine the corresponding kinks in the basis functions.

Second, multicomponent fermions [6] can be treated on an *equal* footing as bosons, only using different basis functions for the segments. In particular, one replaces the cusp condition with the requirement that a basis function must vanish whenever two fermions in the same spin state coincide, $x_i^\sigma = x_{i'}^\sigma$. One can clearly also work with mixtures of fermions and bosons [6].

Third, long-range interactions will couple pairs of segments, changing $\sum_j \hat{U}_j$ to $\sum_{j,j'} \hat{U}_{j,j'}$ in Eq. (4). The simplest case is that of an exponential decay [20], $u(x,x') = e^{-\kappa|x-x'|}$, which yields $\hat{U}_{j,j'} = e^{\kappa\delta(j-j')} \hat{V}_j^+ \hat{V}_{j'}^-$ for segments of equal width δ and $j < j'$, where $\hat{V}_j^\pm$ are weighted averages of the density in segment j. Such exponential terms increase the MPO bond dimension of $\hat{H}$ only by 1 [1]. Power-law interactions, $u(x,x') = f(|x-x'|)|x-x'|^{-\nu}$ where $f(|x|) \to 1$ for large $|x|$, can be approximated by a sum of relatively few exponentials [60,61]. Optimal basis functions can be estimated from the two-body problem as well as exact solutions for $\nu = 2$ [62], which can serve as a benchmark for the nonintegrable cases such as dipolar interactions [63] and Coulomb repulsion [64].

In summary, our cDMRG technique uses spatial partitioning to map a continuous many-body Hamiltonian to discrete DMRG, seemlessly integrating with existing routines: All techniques that accelerate convergence of traditional DMRG calculations [1] (symmetries, state prediction, etc.) carry over. By using physically motivated basis functions, we are able to obtain fast convergence with a limited number of segments, avoiding the need for multiscale optimization [13]. Nonetheless, cDMRG can work in conjunction with such approaches by using the subdividing algorithm illustrated in Fig. 5 (see Supplemental Material for further details [45]). Additionally, our approach may be combined with existing techniques for time evolution, such as the energy-conserving time-dependent variational principle [65], or extended to higher dimensions. This will open exciting applications to unsolved nonequilibrium problems such as prethermalization of strongly interacting bosons [34], domain wall instability in Fermi superfluids [66,67], false vacuum decay in cosmology [68], as well as problems in quantum chemistry [69].

An open-source code is available at Ref. [70].

We thank François Damanet, Stuart Flannigan, and Frank Verstraete for useful discussions. This work was supported by the Engineering and Physical Sciences Research Council Grant No. EP/P009565/1, the National Science Foundation Grants No. PHY-1806357 and No. PHY-2110250, and a Max Planck Society scholarship.

[1] U. Schollwöck, The density-matrix renormalization group in the age of matrix product states, Ann. Phys. (Amsterdam) **326**, 96 (2011).
[2] J. Eisert, M. Cramer, and M. B. Plenio, Colloquium: Area laws for the entanglement entropy, Rev. Mod. Phys. **82**, 277 (2010).
[3] S. Paeckel, T. Köhler, A. Swoboda, S. R. Manmana, U. Schollwöck, and C. Hubig, Time-evolution methods for matrix-product states, Ann. Phys. (Amsterdam) **411**, 167998 (2019).
[4] R. Orús, Tensor networks for complex quantum systems, Nat. Rev. Phys. **1**, 538 (2019).
[5] M. A. Cazalilla, R. Citro, T. Giamarchi, E. Orignac, and M. Rigol, One dimensional bosons: From condensed matter systems to ultracold gases, Rev. Mod. Phys. **83**, 1405 (2011).
[6] X.-W. Guan, M. T. Batchelor, and C. Lee, Fermi gases in one dimension: From Bethe ansatz to experiments, Rev. Mod. Phys. **85**, 1633 (2013).
[7] P. Kunkel, M. Prüfer, S. Lannig, R. Strohmaier, M. Gärttner, H. Strobel, and M. K. Oberthaler, Detecting Entanglement Structure in Continuous Many-Body Quantum Systems, Phys. Rev. Lett. **128**, 020402 (2022).
[8] S. Iblisdir, R. Orus, and J. I. Latorre, Matrix product states algorithms and continuous systems, Phys. Rev. B **75**, 104305 (2007).
[9] T. Sugihara, Density matrix renormalization group in a two-dimensional $\lambda\phi^4$ Hamiltonian lattice model, J. High Energy Phys. 05 (2004) 007.
[10] E. M. Stoudenmire, L. O. Wagner, S. R. White, and K. Burke, One-Dimensional Continuum Electronic Structure with the Density-Matrix Renormalization Group and its Implications for Density-Functional Theory, Phys. Rev. Lett. **109**, 056402 (2012).
[11] M. Knap, C. J. M. Mathy, M. Ganahl, M. B. Zvonarev, and E. Demler, Quantum Flutter: Signatures and Robustness, Phys. Rev. Lett. **112**, 015302 (2014).
[12] F. F. Bellotti, A. S. Dehkharghani, and N. T. Zinner, Comparing numerical and analytical approaches to strongly interacting two-component mixtures in one dimensional traps, Eur. Phys. J. D **71**, 37 (2017).
[13] M. Dolfi, B. Bauer, M. Troyer, and Z. Ristivojevic, Multigrid Algorithms for Tensor Network States, Phys. Rev. Lett. **109**, 020604 (2012).
[14] M. Ganahl and G. Vidal, Continuous matrix product states for nonrelativistic quantum fields: A lattice algorithm for inhomogeneous systems, Phys. Rev. B **98**, 195105 (2018).
[15] R. Haghshenas, Z.-H. Cui, and Garnet Kin-Lic Chan, Numerical continuum tensor networks in two dimensions, Phys. Rev. Research **3**, 023057 (2021).

[16] U. Schollwöck, Progress in density matrix renormalization: What quantum information is teaching us, J. Magn. Magn. Mater. **310**, 1394 (2007).
[17] F. Verstraete and J. I. Cirac, Continuous Matrix Product States for Quantum Fields, Phys. Rev. Lett. **104**, 190405 (2010).
[18] D. Draxler, J. Haegeman, T. J. Osborne, V. Stojevic, L. Vanderstraeten, and F. Verstraete, Particles, Holes, and Solitons: A Matrix Product State Approach, Phys. Rev. Lett. **111**, 020402 (2013).
[19] V. Stojevic, J. Haegeman, I. P. McCulloch, L. Tagliacozzo, and F. Verstraete, Conformal data from finite entanglement scaling, Phys. Rev. B **91**, 035120 (2015).
[20] J. Rincón, M. Ganahl, and G. Vidal, Lieb-Liniger model with exponentially decaying interactions: A continuous matrix product state study, Phys. Rev. B **92**, 115107 (2015).
[21] S. S. Chung and C. J. Bolech, Multiple phase separation in one-dimensional mixtures of mass-and population-imbalanced attractive Fermi gases, Phys. Rev. A **96**, 023609 (2017).
[22] D. Draxler, J. Haegeman, F. Verstraete, and M. Rizzi, Continuous matrix product states with periodic boundary conditions and an application to atomtronics, Phys. Rev. B **95**, 045145 (2017).
[23] M. Ganahl, Continuous matrix product states for inhomogeneous quantum field theories: A basis-spline approach, arXiv:1712.01260.
[24] B. Tuybens, J. De Nardis, J. Haegeman, and F. Verstraete, Variational Optimization of Continuous Matrix Product States, Phys. Rev. Lett. **128**, 020501 (2022).
[25] J. Haegeman, J. I. Cirac, T. J. Osborne, and F. Verstraete, Calculus of continuous matrix product states, Phys. Rev. B **88**, 085118 (2013).
[26] J. Haegeman, D. Draxler, V. Stojevic, J. I. Cirac, T. J. Osborne, and F. Verstraete, Quantum Gross-Pitaevskii equation, SciPost Phys. **3**, 006 (2017).
[27] I. Maruyama and H. Katsura, Continuous matrix product ansatz for the one-dimensional Bose gas with point interaction, J. Phys. Soc. Jpn. **79**, 073002 (2010).
[28] M. Fishman, S. R. White, and E. M. Stoudenmire, The ITensor software library for tensor network calculations, arXiv:2007.14822.
[29] G. Carleo and M. Troyer, Solving the quantum many-body problem with artificial neural networks, Science **355**, 602 (2017).
[30] I. P. McCulloch, From density-matrix renormalization group to matrix product states, J. Stat. Mech. (2007) P10014.
[31] E. H. Lieb and W. Liniger, Exact analysis of an interacting Bose gas. I. The general solution and the ground state, Phys. Rev. **130**, 1605 (1963).
[32] T. Kinoshita, T. Wenger, and D. S. Weiss, Observation of a one-dimensional Tonks-Girardeau gas, Science **305**, 1125 (2004).
[33] T. Kinoshita, T. Wenger, and D. S. Weiss, A quantum Newton's cradle, Nature (London) **440**, 900 (2006).
[34] C. Eigen, J. A. P. Glidden, R. Lopes, E. A. Cornell, R. P. Smith, and Z. Hadzibabic, Universal prethermal dynamics of Bose gases quenched to unitarity, Nature (London) **563**, 221 (2018).
[35] J. J. P. Van Es, P. Wicke, A. H. Van Amerongen, C. Rétif, S. Whitlock, and N. J. Van Druten, Box traps on an atom chip for one-dimensional quantum gases, J. Phys. B **43**, 155002 (2010).
[36] M. Tajik, B. Rauer, T. Schweigler, F. Cataldini, J. Sabino, F. S. Møller, S.-C. Ji, I. E. Mazets, and J. Schmiedmayer, Designing arbitrary one-dimensional potentials on an atom chip, Opt. Express **27**, 33474 (2019).
[37] M. Gaudin, Boundary energy of a Bose gas in one dimension, Phys. Rev. A **4**, 386 (1971).
[38] M. T. Batchelor, X.-W. Guan, N. Oelkers, and C. Lee, The 1D interacting Bose gas in a hard wall box, J. Phys. A **38**, 7787 (2005).
[39] Y. Hao, Y. Zhang, J. Q. Liang, and S. Chen, Ground-state properties of one-dimensional ultracold Bose gases in a hard-wall trap, Phys. Rev. A **73**, 063617 (2006).
[40] L. D. Carr, C. W. Clark, and W. P. Reinhardt, Stationary solutions of the one-dimensional nonlinear Schrödinger equation. I. Case of repulsive nonlinearity, Phys. Rev. A **62**, 063610 (2000).
[41] P. J. Forrester, N. E. Frankel, T. M. Garoni, and N. S. Witte, Painlevé transcendent evaluations of finite system density matrices for 1d impenetrable bosons, Commun. Math. Phys. **238**, 257 (2003).
[42] M. A. Cazalilla, Bosonizing one-dimensional cold atomic gases, J. Phys. B **37**, S1 (2004).
[43] W. Xu and M. Rigol, Universal scaling of density and momentum distributions in Lieb-Liniger gases, Phys. Rev. A **92**, 063623 (2015).
[44] C. Kollath, U. Schollwöck, J. von Delft, and W. Zwerger, One-dimensional density waves of ultracold bosons in an optical lattice, Phys. Rev. A **71**, 053606 (2005).
[45] See Supplemental Material at http://link.aps.org/supplemental/10.1103/PhysRevLett.128.230401, which includes Ref. [46], for a derivation of the partitioned Hamiltonian, generation and splitting of basis states, matrix elements of local operators, details of simulation parameters, convergence of single-particle correlations, numerical strategies, and analysis of approximate models in different limits.
[46] S. Zhang and J. Jin, *Computation of Special Functions* (Wiley, New York, 1996).
[47] M. Olshanii and V. Dunjko, Short-Distance Correlation Properties of the Lieb-Liniger System and Momentum Distributions of Trapped One-Dimensional Atomic Gases, Phys. Rev. Lett. **91**, 090401 (2003).
[48] P. Calabrese, M. Mintchev, and E. Vicari, Entanglement Entropy of One-Dimensional Gases, Phys. Rev. Lett. **107**, 020601 (2011).
[49] C. M. Herdman, P.-N. Roy, R. G. Melko, and A. Del Maestro, Spatial entanglement entropy in the ground state of the Lieb-Liniger model, Phys. Rev. B **94**, 064524 (2016).
[50] C. Simon, Natural entanglement in Bose-Einstein condensates, Phys. Rev. A **66**, 052323 (2002).
[51] F. Pollmann, S. Mukerjee, A. M. Turner, and J. E. Moore, Theory of Finite-Entanglement Scaling at One-Dimensional Quantum Critical Points, Phys. Rev. Lett. **102**, 255701 (2009).
[52] M. Girardeau, Relationship between systems of impenetrable bosons and fermions in one dimension, J. Math. Phys. (N.Y.) **1**, 516 (1960).

[53] T. Stöferle, H. Moritz, C. Schori, M. Köhl, and T. Esslinger, Transition from a Strongly Interacting 1D Superfluid to a Mott Insulator, Phys. Rev. Lett. **92**, 130403 (2004).
[54] H. P. Büchler, G. Blatter, and W. Zwerger, Commensurate-Incommensurate Transition of Cold Atoms in an Optical Lattice, Phys. Rev. Lett. **90**, 130401 (2003).
[55] E. Haller, R. Hart, M. J. Mark, J. G. Danzl, L. Reichsöllner, M. Gustavsson, M. Dalmonte, G. Pupillo, and H.-C. Nägerl, Pinning quantum phase transition for a Luttinger liquid of strongly interacting bosons, Nature (London) **466**, 597 (2010).
[56] G. Boéris *et al.*, Mott transition for strongly interacting one-dimensional bosons in a shallow periodic potential, Phys. Rev. A **93**, 011601(R) (2016).
[57] G. E. Astrakharchik, K. V. Krutitsky, M. Lewenstein, and F. Mazzanti, One-dimensional Bose gas in optical lattices of arbitrary strength, Phys. Rev. A **93**, 021605(R) (2016).
[58] T. Giamarchi, *Quantum Physics in One Dimension* (Oxford University Press, New York, 2003).
[59] P. Calabrese and J. Cardy, Entanglement entropy and quantum field theory, J. Stat. Mech. (2004) P06002.
[60] G. M. Crosswhite, A. C. Doherty, and G. Vidal, Applying matrix product operators to model systems with long-range interactions, Phys. Rev. B **78**, 035116 (2008).
[61] F. Fröwis, V. Nebendahl, and W. Dür, Tensor operators: Constructions and applications for long-range interaction systems, Phys. Rev. A **81**, 062337 (2010).
[62] B. Sutherland, Quantum many-body problem in one dimension: Ground state, J. Math. Phys. (N.Y.) **12**, 246 (1971).
[63] M. A. Baranov, M. Dalmonte, G. Pupillo, and P. Zoller, Condensed matter theory of dipolar quantum gases, Chem. Rev. **112**, 5012 (2012).
[64] J. Schmidt, A. Lambrecht, P. Weckesser, M. Debatin, L. Karpa, and T. Schaetz, Optical Trapping of Ion Coulomb Crystals, Phys. Rev. X **8**, 021028 (2018).
[65] J. Haegeman, C. Lubich, I. Oseledets, B. Vandereycken, and F. Verstraete, Unifying time evolution and optimization with matrix product states, Phys. Rev. B **94**, 165116 (2016).
[66] H. Lu, L. O. Baksmaty, C. J. Bolech, and H. Pu, Expansion of 1D Polarized Superfluids: The Fulde-Ferrell-Larkin-Ovchinnikov State Reveals Itself, Phys. Rev. Lett. **108**, 225302 (2012).
[67] S. Dutta and E. J. Mueller, Collective Modes of a Soliton Train in a Fermi Superfluid, Phys. Rev. Lett. **118**, 260402 (2017).
[68] K. L. Ng, B. Opanchuk, M. Thenabadu, M. Reid, and P. D. Drummond, Fate of the false vacuum: Finite temperature, entropy, and topological phase in quantum simulations of the early universe, PRX Quantum **2**, 010350 (2021).
[69] A. Baiardi and M. Reiher, The density matrix renormalization group in chemistry and molecular physics: Recent developments and new challenges, J. Chem. Phys. **152**, 040903 (2020).
[70] https://github.com/Shovan-Physics/cDMRG.